NATIONAL RADIO ASTRONOMY OBSERVATORY

VLA SCIENTIFIC MEMORANDUM NO. 8

SEPTEMBER 14, 1967

ATMOSPHERIC EFFECTS ON RADIO WAVE PHASE AND THE CORRECTION OF VAPOR-CAUSED PHASE FLUCTUATIONS BY RADIOMETRIC MEASUREMENTS OF WATER VAPOR EMISSION

Joe W. Waters

ABSTRACT

Expressions are obtained for the phase delay of a radio wave as a function of meteorological parameters. Calculations of total water vapor, vapor phase delays, and dry air phase delays are performed from U. S. Weather Bureau radiosonde data for three locations in the Southwest which might resemble locations for large radio telescope arrays and for Huntington, West Virginia, which is the nearest radiosonde station to the radio telescopes at Green Bank. The phase delay due to water vapor is related to the thermal emission of water vapor near its 1.35 cm resonance line. Phase delays predicted from computed water vapor emission spectra are compared with those calculated directly from the radiosonde data.

I. Atmospheric Effects on Radio Wave Phase

A. Theory

The phase change experienced by an electromagnetic wave propagating along a path L is

$$\Delta\phi = \frac{2\pi}{\lambda_0} \int_L n(\ell)\, d\ell \quad \text{radians} \tag{1}$$

where λ_0 is the wavelength in vacuum and $n(\ell)$ is the refractive index at position ℓ on the path. The refractive index of air is usually expressed in N-units where

$$N = (n - 1) \cdot 10^6 \tag{2}$$

and represents, in parts per million, the deviation from unity. For frequencies below 30 GHz N is independent of frequency (the dispersive effect of the 22.2 GHz water vapor resonance line is considered in Appendix 1) and given by [1].

$$N = \frac{77.6}{T}\left(P + \frac{4810\, e}{T}\right) \tag{3}$$

where T = temperature (°K)

P = total pressure (mb.)

e = partial pressure of water vapor (mb.)

Using the relation derived in Appendix 2 relating relative humidity, temperature, and water vapor density, (3) can be written as

$$N = N_d + N_v$$

where

$$N_d = 77.6 \frac{P}{T} = 2.7 \times 10^4 \rho_d \quad \text{due to dry air} \tag{4a}$$

$$N_v = 1.723 \times 10^3 \frac{\rho_v}{T} \quad \text{due to water vapor} \tag{4b}$$

In equations (4), ρ_d and ρ_v are respectively the dry air density and water vapor density expressed in grams per cubic meter. The physical reason that the index of refraction of water vapor is proportional to density divided by temperature whereas that of dry air is proportional to density is that the water vapor molecule has an electric dipole moment. The random alignment of the dipole increases with temperature thus lowering the index of refraction. Typical values of N_d and N_v in the lower troposphere are for frequencies below 30 GHz

$$N_d \approx 250$$

$$N_v \approx 50.$$

Combining equations (1), (2), and (4), expressions are obtained for the additional phase delay introduced by the atmosphere on a wave propagating along path L.

$$\Delta\phi_d = \frac{2\pi}{\lambda_0} \cdot 77.6 \times 10^{-6} \int_L \frac{P}{T}\, d\ell \text{ radians} \qquad \text{due to dry air} \qquad (5a)$$

$$= \frac{2\pi}{\lambda_0} \cdot 2.7 \times 10^{-2} \int_L \rho_d\, d\ell \text{ radians}$$

$$\Delta\phi_v = \frac{2\pi}{\lambda_0} \cdot 1.723 \times 10^{-3} \int_L \frac{\rho_v}{T}\, d\ell \text{ radians} \qquad \text{due to vapor} \qquad (5b)$$

The integrals in equations (5) must be taken over the exact path traveled by the wave including refractive bending of the path by the atmosphere. Bending is considered below.

One may relate the total vapor phase delay to the total precipitable water vapor by defining an effective temperature $\overline{T}$ such that

$$\int_L \frac{\rho_v}{T}\, d\ell = \frac{1}{\overline{T}} \int_L \rho_v\, d\ell$$

Then

$$\Delta\phi_v = \frac{108}{\lambda_0} \frac{M_v}{\bar{T}} \quad \text{radians} \tag{6}$$

where M_v = total precipitable water vapor in cm.

Equation (6) can be made independent of frequency by expressing the phase delay as an increase in path length ΔL_v

$$\Delta L_v = \frac{\lambda_0}{2\pi} \Delta\phi_v = 17.2 \frac{M_v}{\bar{T}} \quad \text{meters}$$

Assuming $\bar{T} = 280\ ^\circ K$ leads to

$$\frac{\Delta L_v}{M_v} = 6.1 \quad \frac{\text{cm path length increase}}{\text{cm precipitable water vapor}}$$

as the relation between the path length increase and the amount of precipitable water vapor.

An estimate of the lengthening of the geometrical path due to bending is obtained using Schulkin's [2] calculation shown in figure 1 for total atmospheric bending. To first order the difference between the actual bent path L and the apparent path L' (see figure 2) is

$$\Delta L_{bending} = \frac{h_0 \Delta\Theta(\Theta_0)}{\sin\Theta_0 \tan\Theta_0}$$

where h_0 is an effective height of the atmosphere and $\Delta\Theta(\Theta_0)$ is the total bending at angle Θ_0 with the horizon. Equation (7) holds only for $\Theta_0 \gtrsim 10°$. For $\Theta_0 = 10°$ and using $h_0 = 10$ km

$$\Delta L_{bending} = 326 \text{ meters}$$

At 11 cm wavelength this corresponds to a phase delay of

$$\Delta\phi_{\text{bending}} = 1.86 \times 10^{4} \text{ radians.}$$

B. Calculations from Radiosonde Data

Figures 3-6 show the results of evaluating the integrals of equations (5) for atmospheric conditions as determined from U.S. Weather Bureau radiosondes launched at twelve hour intervals. The phase delays due to vapor and dry air are plotted separately on the lower portion of the graphs with total water vapor indicated on the upper portion. The phase calculations are for a signal at 11 cm wavelength propagating vertically down through the atmosphere, so that bending effects are not present. All integrals were evaluated between the surface level and a height corresponding to 100 mb pressure (approximately 16.5 kilometers). Trapezoidal integration of the radiosonde data points was used. The height difference between data points was approximately 0.5 kilometers.

Results of calculations are shown for three locations in the southwestern United States, which might resemble potential sites for a large array of radio telescopes, and for Huntington, West Virginia, which is the nearest radiosonde station to the radio telescopes at Green Bank. The dates used are the first five days of February and of August to illustrate the extremes of seasons. Some statistical information is obtained since the calculations are performed for each of the past five years (1962-66). Statistics for total water vapor as determined from the data presented in figures 3-6 are given in table 1. The stations are arranged in order of the five year average of the standard deviation.

Mean atmospheric water vapor density and relative humidity profiles are shown in figure 7 for February and August for each of the locations. Although the surface value of the relative humidity is appreciably lower for three stations in the southwest, the amount of water vapor at these stations is not as significantly lower due to their warmer climate. Relative humidity can be a misleading measure of water vapor density because the absolute amount of vapor that air can hold increases with temperature.

TOTAL WATER VAPOR STATISTICS

all values in cm of total precipitable water

Station	1962		1963		1964		1965		1966		5-Year Average	
	mean	σ	mean	σ	mean	σ	mean	σ	mean	σ	mean	σ
	February 1-5											
El Paso	.59	.10	.91	.19	.50	.10	.91	.18	.63	.11	.75	.18
Albuquerque....	.60	.09	.96	.27	.43	.13	.57	.18	.56	.06	.67	.19
Tucson	.70	.07	1.32	.36	.52	.12	1.21	.36	.76	.18	.95	.30
Huntington	1.28	.30	1.29	.84	.70	.36	.37	.23	.60	.18	.89	.43
	August 1-5											
Albuquerque....	1.79	.41	2.37	.29	2.47	.39	2.33	.27	2.71	.36	2.38	.39
Tucson	2.84	.72	4.03	.26	3.84	.35	2.84	.52	3.60	.30	3.48	.48
El Paso	2.69	.44	2.88	.41	2.38	.47	2.44	.48	3.23	.74	2.77	.55
Huntington	3.01	.59	3.16	.57	3.50	.79	2.47	.67	2.59	.67	2.99	.66

Table 1 — Total Water Vapor Statistics showing Mean and Standard Deviation σ.

The errors in the data of figures 3-7 should be less than 5 percent for all values. The U. S. Weather Bureau radiosonde instrumentation consists of a relative humidity sensor and a temperature sensor. Readings are taken at fixed pressure intervals. Height is computed from pressure and temperature. Water vapor density is calculated from relative humidity and temperature as discussed in Appendix 1. The radiosonde relative humidity sensor is a moisture sensitive resistor which gives readings accurate to within 5 percent. This leads to at most a 5 percent error in the total water vapor and vapor phase shift calculated from the radiosonde records. The radiosonde temperature sensor is accurate to a few tenths centigrade degree.

The calculations from radiosonde data discussed above cannot give quantitative predictions of the atmospheric effect on phase stability of an array of radio telescopes. For the operation of such an array one is interested not in the total phase shift due to the atmosphere, but how this phase shift varies from the line of sight of one element to another and over a time period comparable to the integration time of the instruments. A measure of both spatial and temporal variation of atmospheric inhomogeneities is necessary before an estimate can be made of this differential phase shift. At the time of writing an accurate value of this correlation distance was not available. Kaydanovskiy and Smirnova [3] use a correlation radius of 60 meters for atmospheric inhomogeneities and conclude that tropospheric effects on phase fluctuations are completely negligible for wavelengths longer than a few centimeters. This conclusion appears extremely optimistic considering the magnitude of phase fluctuations given in figures 3-6. It should be remembered, however, that the sample time for the points shown in these figures is twelve hours. Over a shorter time period, less scatter in the points would be expected.

An infrared device for measuring total precipitable water is now becoming operational at Green Bank. With two of these devices, much information about the structure of atmospheric water vapor cells can be obtained by operating these devices at various baselines and synchronously recording their outputs. A quantitative value for the differential vapor phase shifts can be had by using equation (6) and letting M_v be the difference in total vapor along the two paths.

The phase delay due to liquid water in the atmosphere has been neglected in the analysis so far. Whether or not this is justifiable depends on local conditions. The refractive index of liquid water is shown in figure 8. The points in the centimeter range are values given by Goldstein [4]. At a wavelength of 11 cm the refractive index of 9 leads to the relation between electrical path length increase due to liquid water and total amount of liquid water in path:

$$\frac{\Delta L_{\ell}}{M_{\ell}} = 9 \quad \frac{\text{cm path length increase}}{\text{cm liquid water}} \tag{8}$$

The electrical path length increase due to a cloud of one kilometer dimension (a very wet cloud) containing 1 gm/m^3 liquid water is 9 mm. At 11 cm wavelength this corresponds to approximately thirty degrees phase shift. Data on local cloud conditions are needed in order to obtain quantitative estimates of phase delay due to liquid water.

Water, in both liquid and vapor form, is expected to be the chief cause of phase fluctuations in interferometric systems due to atmospheric turbulence. Although the calculations from radiosonde data indicate that the magnitude of phase fluctuations along a single path due to dry air may be comparable to those due to vapor, the spatial extent of dry air inhomogeneities is expected to be much larger than the dimensions of any feasible array and should not appreciably affect phase stability. More data on dry air inhomogeneities are needed to verify this. The phase delay due to refractive bending becomes important only at angles near the horizon. For these angles, each element of an array will be looking through the same amount of atmosphere and the bending effect should be the same for each.

II. Correction of Phase Fluctuations Due to Atmospheric Water by Radiometric Measurements

In this section the phase delay due to atmospheric water is related to its thermal emission. By radiometrically measuring the emission as seen at various elements of an array one can infer the phase shift due to the atmosphere and make corrections for

different changes along the line of sights of different elements. Ideally the same portion of atmosphere should be contained within the antenna beams of the main array elements and the antenna beam used in measuring the atmospheric water emission.

The brightness temperature at frequency ν due to water vapor is

$$T_B(\nu) = \int_L T(\ell)\alpha_{vapor}(\nu, \ell)\, e^{-\tau(\nu, \ell)}\, d\ell \qquad (9)$$

where ℓ = position along radiation path L

$T(\ell)$ = temperature at ℓ

$\tau(\nu, \ell)$ = opacity at ℓ and frequency ν = $\int_0^{\ell} \alpha_{vapor}(\nu, \ell)\, d\ell$

$\alpha_{vapor}(\nu, \ell)$ is the absorption coefficient of water vapor at frequency ν and for atmospheric conditions at ℓ.

A theoretical expression for the water vapor absorption coefficient was derived from quantum mechanics by Van Vleck in 1947 [5]. The water vapor molecule has a rotational resonance line in the microwave range at 1.35 cm (22.235 GHz) and absorption in the region of this wavelength is greatly enhanced. Due to pressure broadening in the troposphere, the line width is approximately 4 GHz and varies according to the distribution of water vapor with altitude. Atmospheric water vapor spectra have been computed by Hogg [6], Barrett and Chung [7], Staelin [8], and Gaut [9]. Barrett and Chung predict that an anomalous spike will occur in the spectrum at 22.235 GHz due to stratospheric water vapor. Staelin and Gaut compare computed atmospheric opacity spectra with that determined experimentally.

Figure 9 shows brightness temperature and opacity spectra computed for the three locations in the Southwest and Huntington. Spectra are shown for 1966 mean atmospheric conditions for February and August as determined from radiosonde data. Any spikes due to stratospheric water vapor are not present in these calculations as the radiosondes were not capable of detecting vapor in the stratosphere.

The absorption coefficient, $\alpha(\nu, \ell)$ used in computing the spectra of figure 9 was taken from Staelin [8]:

$$\alpha_{vapor}(\nu, \ell) = 3.24 \times 10^{-4} e^{-644/T}$$

$$\frac{\nu^2 P \rho}{T^{3.125}} \left(1 + 0.0147 \frac{\rho T}{P}\right)$$

$$\left[\frac{1}{(\nu - 22.235)^2 + (\Delta\nu)^2}\right.$$

$$\left. + \frac{1}{(\nu + 22.235)^2 + (\Delta\nu)^2}\right]$$

$$+ 2.55 \times 10^{-8} \rho \nu^2 \frac{\Delta\nu}{T^{3/2}} \text{ cm}^{-1} \qquad (11)$$

where

$$\Delta\nu = 2.58 \times 10^{-3} \times \left(1 + 0.0147 \frac{\rho T}{P}\right) \frac{P}{(T/318)^{0.625}}$$

and

ν = frequency, GHz

T = temperature, °K at ℓ

P = total pressure, mb at ℓ

ρ = water vapor density, g/m^3 at ℓ

A plot of $\alpha_{vapor}(\nu, \ell)$ expressed in db/km for $\rho = 1$ gm/m^3, T = 318 °K and P = 1013 mb is shown in figure 10. To a very good approximation $\alpha(\nu, \ell)$ is proportional to ρ, the water vapor density. Also shown in figure 10 are the experimental values determined for the same conditions by Becker and Autler [10].

The problem now is to relate the vapor brightness spectrum to the vapor phase shift. From equation (5b) it is seen that the meteorological quantity which must be determined is $\int (\rho_v/T) d\ell$. Equation (9) can be written as

$$T_B(\nu) = \int_L WF(\nu, \ell) \frac{\rho}{T} d\ell \tag{12}$$

where

$$WF(\nu, \ell) = T^2(\ell) \frac{\alpha(\nu, \ell)}{\rho(\ell)} e^{-\int_0^{\ell} \alpha(\nu, \ell') d\ell'} \tag{13}$$

Equation (10 must be solved for $\int_L \frac{\rho}{T} d\ell$. In order to do this we must have some knowledge of the weighting function $WF(\ell, \nu)$. Figure 11 shows weighting functions at various frequencies near the water vapor resonance line computed for mean December atmospheric conditions over Washington, D. C.

To eliminate non-water vapor contributions, $T_B(\nu)$ can be measured at two frequencies near the 1.35 cm resonance and the difference taken.

$$\Delta T_B(\nu_1, \nu_2) = T_B(\nu_1) - T_B(\nu_2)$$

$$= \int_L [WF(\nu_1, \ell) - WF(\nu_2, \ell)] \frac{\rho}{T} d\ell \tag{14}$$

To a good approximation

$$\frac{\rho}{T} = \frac{\rho_0}{T_0} e^{-kh} \tag{15}$$

where ρ_0, T_0 are surface values

$\frac{1}{k}$ is an effective scale height

h is height above surface.

In the region 0-6 km containing most of the water vapor, the weighting functions are approximately linear with height.

$$WF(\nu, \ell) = a(\nu) + b(\nu)h \tag{16}$$

where $a(\nu)$, $b(\nu)$ are constants for a given frequency.

Combining (14), (15), and (16) with $\ell = h \sec \Theta$, where Θ is the angle of observation with respect to the zenith, yields

$$\Delta T_B(\nu_1, \nu_2) = \frac{\rho_0}{T_0} \int_0^\infty [(a_1 - a_2) + (b_1 - b_2)\, h \sec \Theta]\, e^{-kh} \sec \Theta \, dh$$

$$= \frac{\rho_0}{T_0} \left[\frac{(a_1 - a_2)}{k} \sec \Theta + \frac{(b_1 - b_2) \sec^2 \Theta}{k^2} \right]$$

The above may be solved for k

$$k = \left\{ \frac{\rho_0 (a_1 - a_2)}{2\, T_0\, \Delta T_B} + \sqrt{\left[\frac{\rho_0 (a_1 - a_2)}{2\, T_0\, \Delta T_B} \right]^2 + \frac{\rho_0 (b_1 - b_2)}{T_0\, \Delta T_B}} \right\} \sec \Theta \tag{17}$$

Only the positive root has been retained due to physical considerations.

The vapor phase change is now related to k

$$\Delta \phi_V = \frac{2\pi}{\lambda_0}\, 1.723 \times 10^{-3} \int \frac{\rho}{T}\, d\ell$$

$$= \frac{1.083 \times 10^{-2}}{\lambda_0} \frac{\rho_0}{T_0} \int e^{-kh} \sec \Theta \, dh$$

$$= \frac{1.083 \times 10^{-2}}{\lambda_0} \frac{\rho_0 \sec \Theta}{T_0 k} \text{ radians} \tag{18}$$

Combining (17) and (18)

$$\Delta\phi_v = 2.166 \times 10^{-2} \frac{\Delta T_B}{\lambda_0(a_1 - a_2)} \left\{ \frac{1}{1 + \sqrt{1 + \frac{4\, T_0\, \Delta T_B (b_1 - b_2)}{\rho_0 (a_1 - a_2)^2}}} \right\} \quad (19)$$

Typically, the quantity

$$\frac{4T_0\, \Delta T_B}{\rho_0} \quad \frac{(b_1 - b_2)}{(a_1 - a_2)^2}$$

is of order unity and the bracketed factor in (19) cannot be simplified by an approximation.. Equation (19) relates the vapor phase delay to (1) the difference in brightness temperature at two frequencies, (2) the surface value of the vapor density, temperature, and weighting function, and (3) the effective slope of the weighting function. All of these quantities except the weighting function slope are directly measurable. Equation (19) may be rewritten as

$$\Delta\phi_v = 2.166 \times 10^{-2} \frac{\Delta T_B}{\lambda_0(a_1 - a_2)} \frac{1}{1 + \sqrt{1 + \beta \frac{T_0\, \Delta T_B}{\rho_0}}} \quad (20)$$

where β is a constant depending on the frequencies at which ΔT_B is measured. Although β may be calculated directly from the weighting functions, a more accurate procedure is to use a model atmosphere to calculate all the quantities except β in the above expression and solve for β.* Doing this

$$\beta = \frac{\rho_0}{T_0\, \Delta T_B} \left\{ \left[\frac{21.66\, \Delta T_B}{\Delta\phi_v\, \lambda_0 (a_1 - a_2)} - 1 \right]^2 - 1 \right\} . \quad (21)$$

---

* In retrospect, a more stable expression for $\Delta\phi_v$ would have been obtained if the surface contribution to β had been separated from the contribution due to weighting function slope, namely to have used equation (19) and solved for $(b_1 - b_2)$ from a model atmosphere.

Figure 12 shows the absolute and percentage errors experienced in predicting the vapor phase delay using (20). The correct vapor phase delay is taken as that calculated from (5b). The frequencies used in determining ΔT_B were 20.0 and 22.0 GHz and ΔT_B calculated by evaluating the integral in (9) for individual radiosonde records. The parameter β was calculated from (21) using the February 1966 hour 0 mean atmosphere for February calculations and the August 1966 hour 0 mean atmosphere for August calculations. The errors shown in figure 12 are due only to variations in atmospheric conditions from the model atmosphere used in calculating β. In particular, the errors are due to the difference in the weighting functions for the individual days of calculation and the weighting functions for the model atmosphere. As can be seen from (13) and noting that (a) α/ρ is virtually independent of ρ and (b) $\int \alpha(\nu, \ell)\, d\ell$ is much less than unity except for angles near the horizon, the weighting functions are very insensitive to variations in $\rho(\ell)$. They are most sensitive to variations in the temperature profile $T(\ell)$. The percentage errors when predicting phase variations along different, but nearby, atmospheric paths are expected to be much smaller than those shown in figure 12. Over any feasible array dimension, the temperature will vary by a minute amount and errors due to changes in atmospheric conditions from those of the model used in calculating β should essentially cancel when the difference in phase along two paths is predicted.

Other errors will arise in practice because of errors in measuring ΔT_B and errors in the expression used for the absorption coefficient. From the discrepancy between experimental and theoretical values of $\alpha(\nu, \ell)$ shown in figure 10, the absorption coefficient error may be estimated roughly as 5 percent. More experimental values for $\alpha(\nu, \ell)$ under various conditions are needed before an accurate estimate can be made of this error. The error due to noise in measurements of ΔT_B is straightforwardly determined. From (20) one obtains

$$\frac{d(\Delta\phi_v)}{\Delta\phi_v} = \frac{d(\Delta T_B)}{\Delta T_B} \left\{ 1 - \frac{0.5\, k_2\, \Delta T_B}{1 + k_2\, \Delta T_B + \sqrt{1 + k_2\, \Delta T_B}} \right\}$$

where

$$k_2 = \beta \frac{T_0}{\rho_0}$$

as the relation between the relative errors in ΔT_B and $\Delta \phi_v$. For August conditions in Tucson and frequencies 20 and 22 GHz

$$\Delta T_B = 30$$
$$k_2 = 2.3 \times 10^{-2}$$

which leads to

$$\frac{d(\Delta \phi_v)}{\Delta \phi_v} = .88 \frac{d(\Delta T_B)}{\Delta T_B}$$

For these conditions the percentage error in the phase prediction is slightly less than that in measuring ΔT_B.

The effect of clouds is now considered. The absorption coefficient of clouds valid in the wavelength range 0.8 - 3.0 cm is given by Staelin [8] as

$$\alpha_{clouds} = \frac{10^{0.0122\,(291 - T) - 6}}{\lambda^2} \rho_\ell \quad cm^{-1}$$

where ρ_ℓ is the liquid water density of the clouds in gm/m^3

T is the cloud temperature (°K)

λ is the wavelength (cm)

The total opacity $\int_L \alpha(\nu, \ell)\, d\ell$ is

$$\tau = \frac{10^{0.0122\,(291 - T) - 6}}{\lambda^2} \int \rho_\ell \, d\ell$$

$$= \frac{10^{.0122\,(291 - T) - 2}}{\lambda^2} M_\ell \qquad (23)$$

where M_ℓ is the total amount of liquid water in the clouds in gm/cm^2 and it has been assumed the temperature of the cloud is constant.

The brightness temperature of the clouds is

$$T_{B_{cloud}}(\nu) = \int_0^{\tau} T_{cloud}(\ell)\, e^{-\tau(\nu,\,\ell)}\, d\tau(\nu,\ell) = T_{cloud}(1 - e^{-\tau})$$

for a constant temperature T_{cloud} within the cloud. For opacity τ small compared to unity the above becomes

$$T_{B_{cloud}}(\nu) = T_{cloud}\,\tau(\nu)$$

$$= T_{cloud}\,\frac{10^{.0122\,(291 - T) - 6}}{\lambda^2}\,M_{\ell}$$

The relation between total liquid water and difference in brightness temperatures due to clouds measured at two wavelengths is

$$M_{\ell} = \frac{\Delta T_{B_{cloud}}}{T_{cloud}\left(\frac{1}{\lambda_1^2} - \frac{1}{\lambda_2^2}\right)} \cdot 10^{6 - .0122\,(291 - T)}$$

The phase change due to the liquid water is found from M_{ℓ} by using (8). The brightness temperature due to a one kilometer cloud at temperature 291 °K with 1 gm/m^3 liquid water density is

$$T_{B_{cloud}} = 16.4\ ^{\circ}K \quad \text{at} \quad 22.0\ \text{GHz}.$$

$$T_{B_{cloud}} = 13.5\ ^{\circ}K \quad \text{at} \quad 20.0\ \text{GHz}.$$

Because the spectrum of clouds has a frequency squared dependence, their contribution to the total brightness temperature may be separated from that of water vapor. Staelin gives a method for doing this by choosing frequencies such that the weighting function at the two frequencies are related by

$$WF(\nu_2, \ell) = A \cdot WF(\nu_1, \ell)$$

where A is a constant $\neq \left(\frac{\nu_2}{\nu_1}\right)^2$

Local cloud data is needed before it can be determined if the effects of clouds on phase and emission spectra must be taken into account.

III. Conclusions and Suggestions for Further Work

The zenith phase delay at 11 cm wavelength because of the atmosphere approximately 100 radians due to dry air and 1-10 radians due to water vapor depending upon season. Daily fluctuations are of order 1 radian due to dry air and .5-5 radians due to vapor. More data on atmospheric inhomogeneities is needed before a quantitative estimate can be made of atmospheric effects on the relative phase delays of signals propagating along slightly different paths. It is expected that only water vapor and water droplets have inhomogeneity scale sizes sufficiently small to affect the phase performance of an array of feasible dimensions.

Although surface values of relative humidity are appreciably lower in the southwestern U.S. than in West Virginia, the amount and daily fluctuations in total vapor and vapor phase delays are of the same order for both regions.

By measuring the thermal emission from atmospheric water vapor near the 1.35 cm resonance line, the phase delay due to the vapor can be predicted. Using a derived expression relating vapor phase delay and brightness temperature difference at two frequencies, vapor phase delays were predicted which always agreed within twenty percent and usually within ten percent of the exact value for all cases considered. In the cases for which the model atmosphere used in calculating weighting function constants was appropriate (namely those for hour 0, 1966) agreement was always within five percent. The major source of error in these calculations is the temperature variation in the atmosphere. The relative errors should be significiantly less in predicting relative phase differences along slightly different paths.

Another method for predicting phase delays from emission spectra is the optimum linear inversion technique developed by Staelin [11] and applied to the atmospheric water vapor problem by Gaut [9] and Gaut, Barrett and Staelin [12]. Their results indicate that the total amount of water vapor can be predicted to approximately 1 percent accuracy with this method. However, the data used in making the predictions consisted of an absolute value of atmospheric opacity at five frequencies. A measurement of opacity is much more difficult to perform than that of the difference in brightness temperature at two frequencies required for the inversion technique used in this paper. At the time of writing, the author had not successfully applied the optimum linear inversion technique to the problem of estimating total water vapor and vapor phase delays from a measurement of the difference in brightness temperature at two frequencies. This work is being continued.

Suggestions for further work in the problem of phase fluctuations due to atmospheric turbulence are: (1) Putting into operation a system of two or more infrared hygrometers at various baselines to determine the fluctuations in water vapor over slightly different paths. From these measurements one can tell whether or not a correction is needed for vapor-caused phase fluctuations, provided the infrared instruments accurately measure the water vapor content. (2) A study of the limitations of the infrared hygrometers due to cloud coverage and calibration accuracy. (3) A study of the possibility of building an infrared device sensitive enough to detect the water vapor in emission, rather than absorption against the sun as is now being done. If this proves possible, the problem of predicting phase fluctuations from infrared emission measurements should be considered. (4) Construction of two radiometers operating near the 1.35 cm water vapor resonance for predicting vapor-caused phase fluctuations and comparing with or correcting for the phase fluctuations in the NRAO interferometer at Green Bank.

References

[1] Bean, B.R., and E. J. Dutton, Radio Metorology, National Bureau of Standards Monograph 92.

[2] Schulkin, M., "Average Radio Ray Refraction in the Lower Atmosphere," Proc. IRE, Vol. 40, No. 5, 554-561 (May 1952).

[3] Kaydanovskiy, N. L., and N. A. Smirnova, "Resolution Limits of Radio Telescopes and Radio Interferometers Imposed by Propagation of Waves in the Space and in the Atmosphere of the Earth," Radio Engrg. Electronic Physics (USA), Vol. 10, No. 9, pp. 1355-62 (Sept. 1965).

[4] Goldstein, Herbert, "Attenuation by Condensed Water," in Propagation of Short Radio Waves edited by D. E. Kerr, McGraw Hill (1951).

[5] Van Vleck, J. H., "The Absorption of Microwaves by Uncondensed Water Vapor," Physical Review, Vol. 71, No. 7, pp. 425-433 (April 1, 1967).

[6] Hogg, D. C., "Effective Antenna Temperatures Due to Oxygen and Water Vapor in the Atmosphere," Journal of Applied Physics, Vol. 30, No. 9, pp. 1417-1419 (Sept. 1959).

[7] Barrett, A. H., and V. K. Chung, "A Method for the Determination of High Altitude Water Vapor Abundance from Ground Based Microwave Observations," Journal of Geophysical Research, Vol. 67, No. 11, pp. 4259-4266 (Sept. 1962).

[8] Staelin, D. H., " Measurements and Interpretation of the Microwave Spectrum of the Terrestrial Atmosphere Near 1-Centimeter Wavelength," Journal of Geophysical Research, Vol. 71, No. 12, pp. 2875-2881 (June 15, 1966).

[9] Gaut, N. E., "Studies of Atmospheric Water Vapor by Means of Passive Microwave Techniques," Ph.D. thesis, Massachusetts Institute of Technology, 1967.

[10] Becker, G. E., and S. H. Autler, "Water Vapor Absorption of Electromagnetic Radiation in the Centimeter Wave-Length Range," Physical Review, Vol. 70, Nos. 5 and 6 (1946).

[11] Staelin, D. H., The Detection and Measurement of Radio Astronomical Signals, notes for MIT subject 6.624 (1967).

[12] Gaut, N. E., A. H. Barrett, D. H. Staelin, "Results Obtained from the Inversion of Simulated Atmospheric Water Vapor Spectra," Quarterly Progress Report, MIT, RLE, April 15, 1967, pp. 16-19.

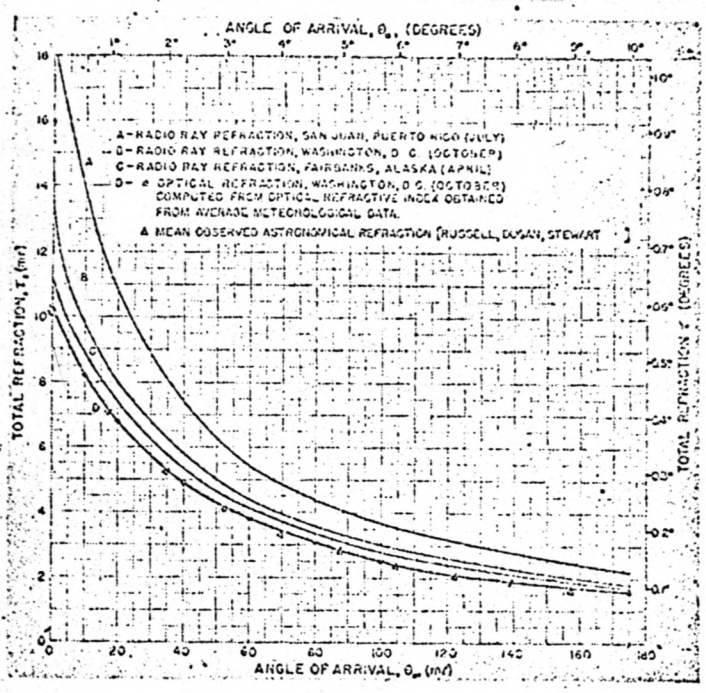

Total refraction versus angle of arrival, $\theta_0 \leqq 10°$.

(a)

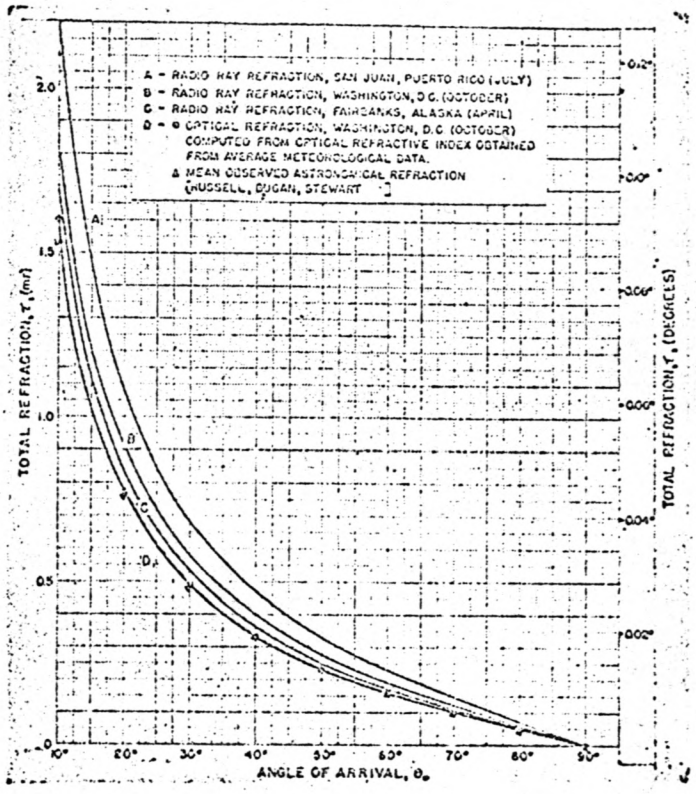

—Total refraction versus angle of arrival, $\theta_0 \geqq 10°$.

(b)

Fig. 1 — Total bending due to atmosphere (from Shulkin)

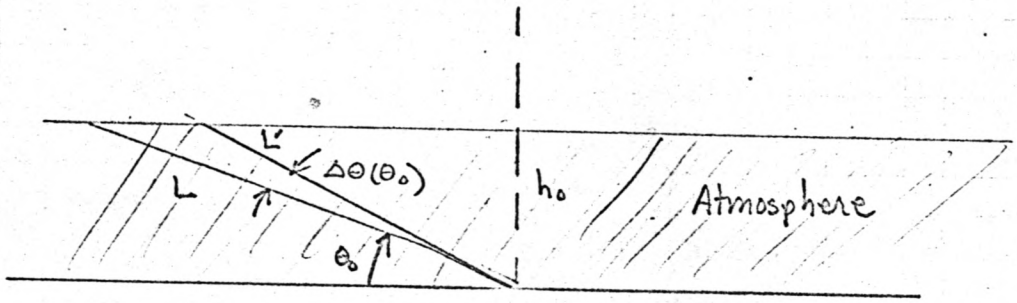

Fig. 2 — For calculating increase in geometrical path due to atmospheric bending.

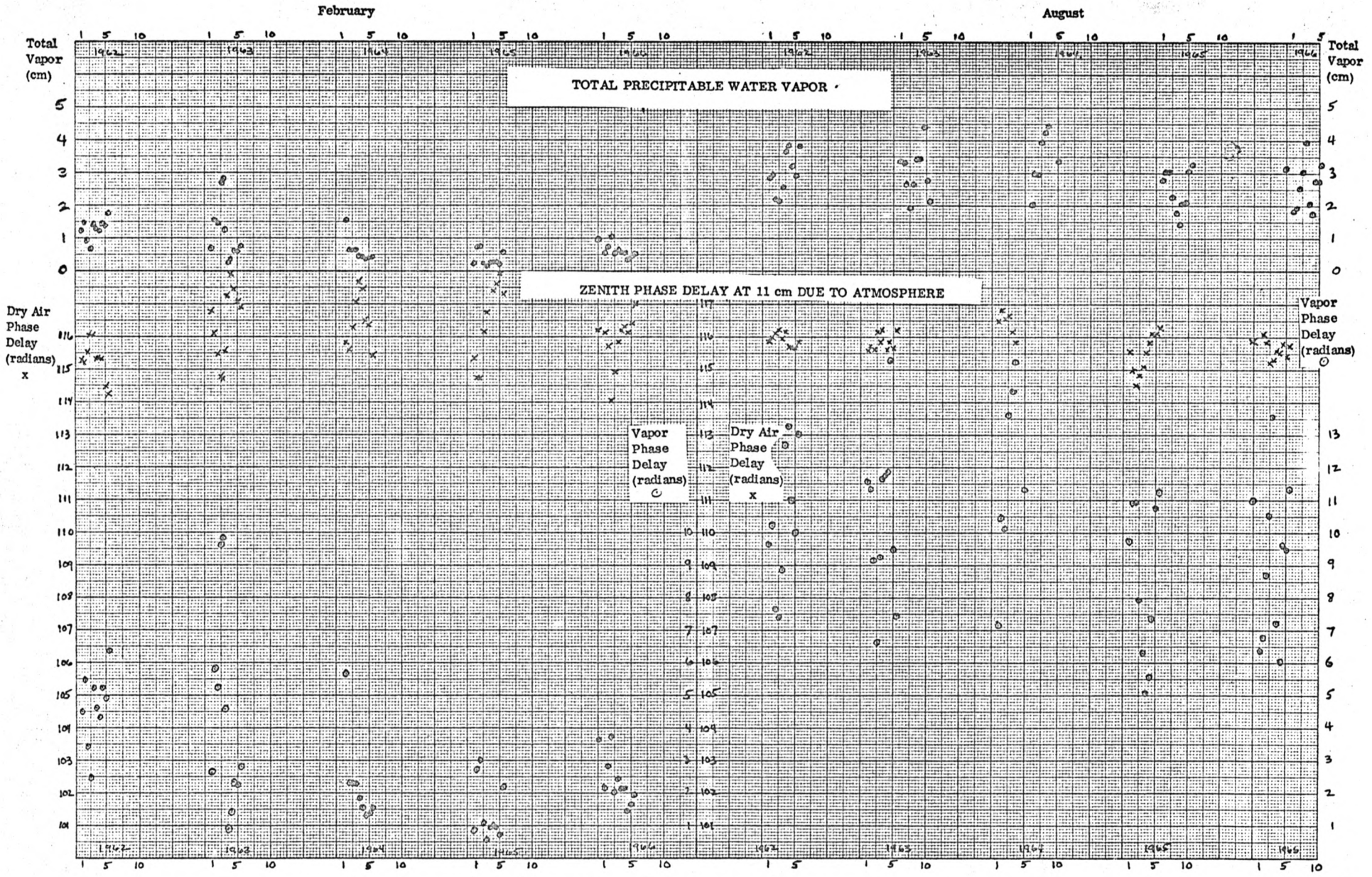

Fig. 3 — Results of Radiosonde Data from Huntington, W. Va.

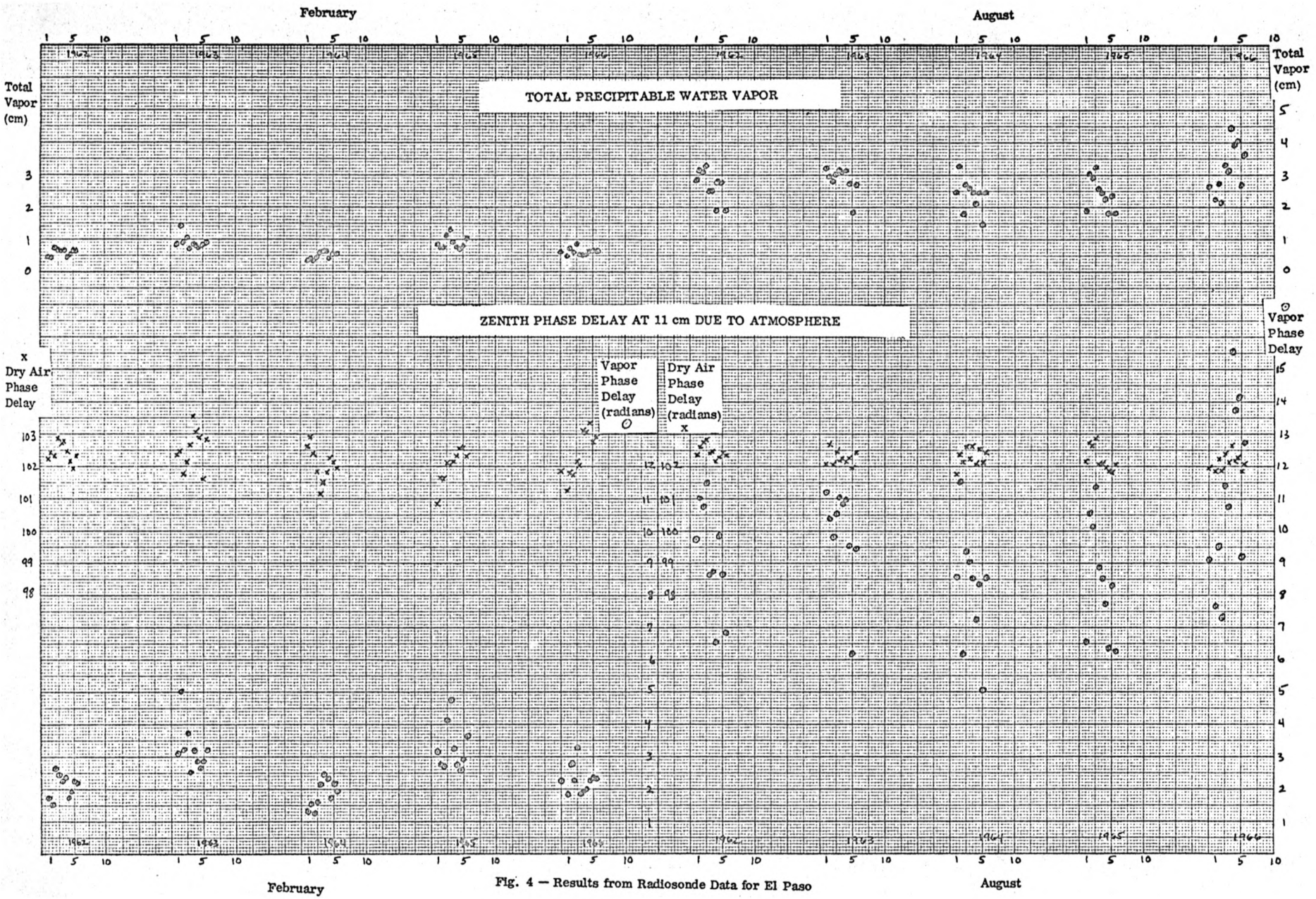

Fig. 4 — Results from Radiosonde Data for El Paso

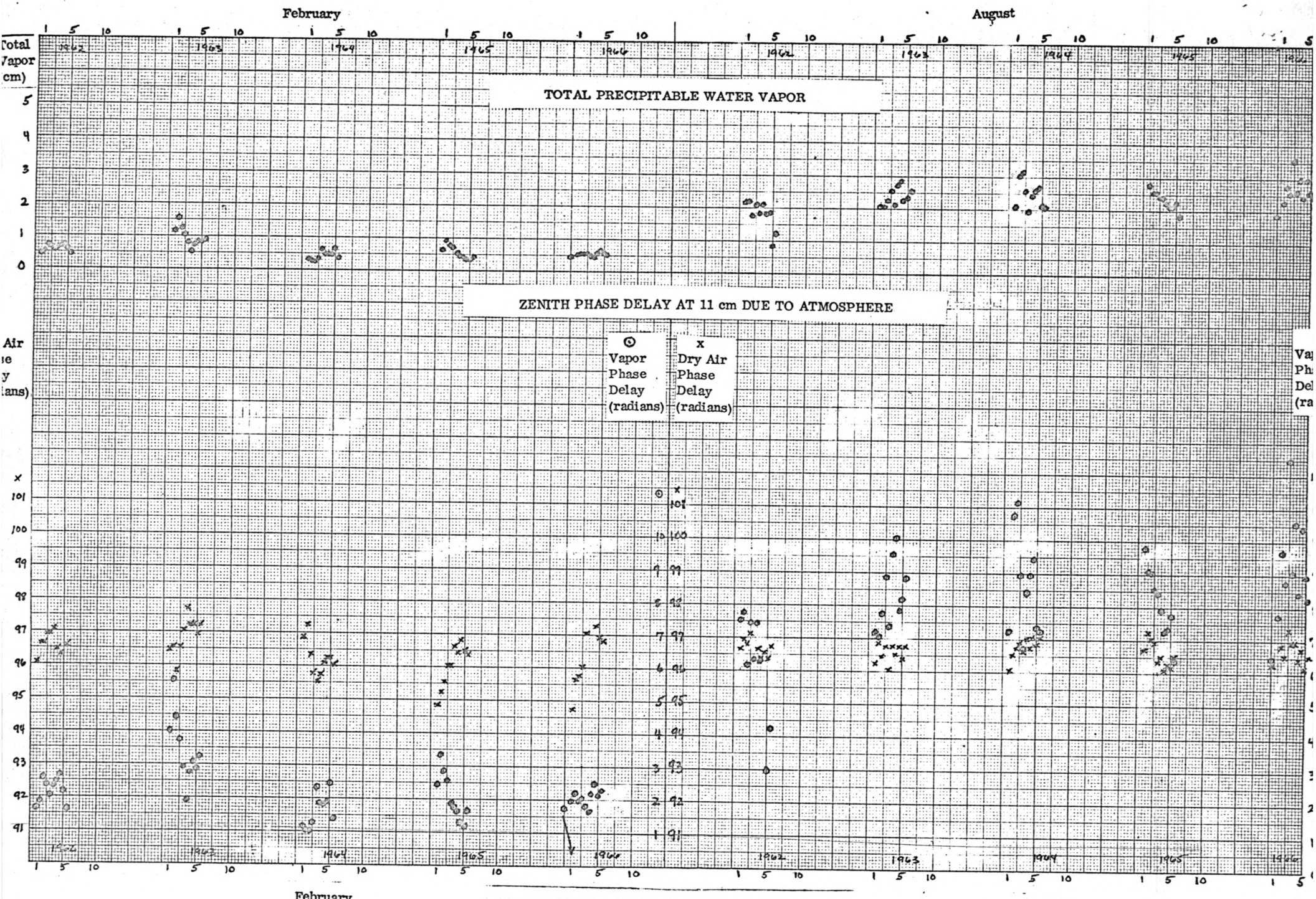

Fig. 5 — Results of Radiosonde Data from Albuquerque

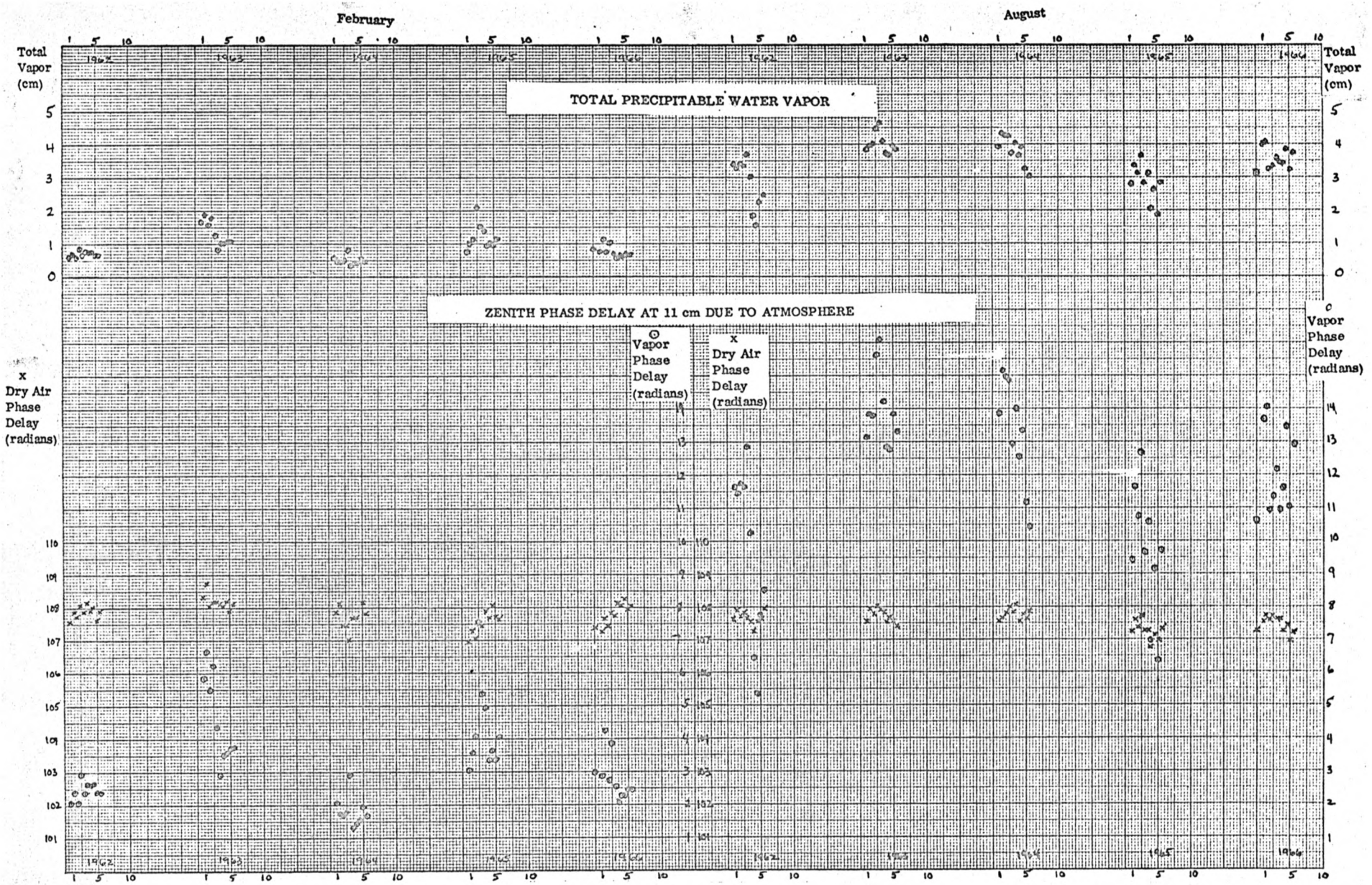

Fig. 6 — Results from Radiosonde Data for Tucson

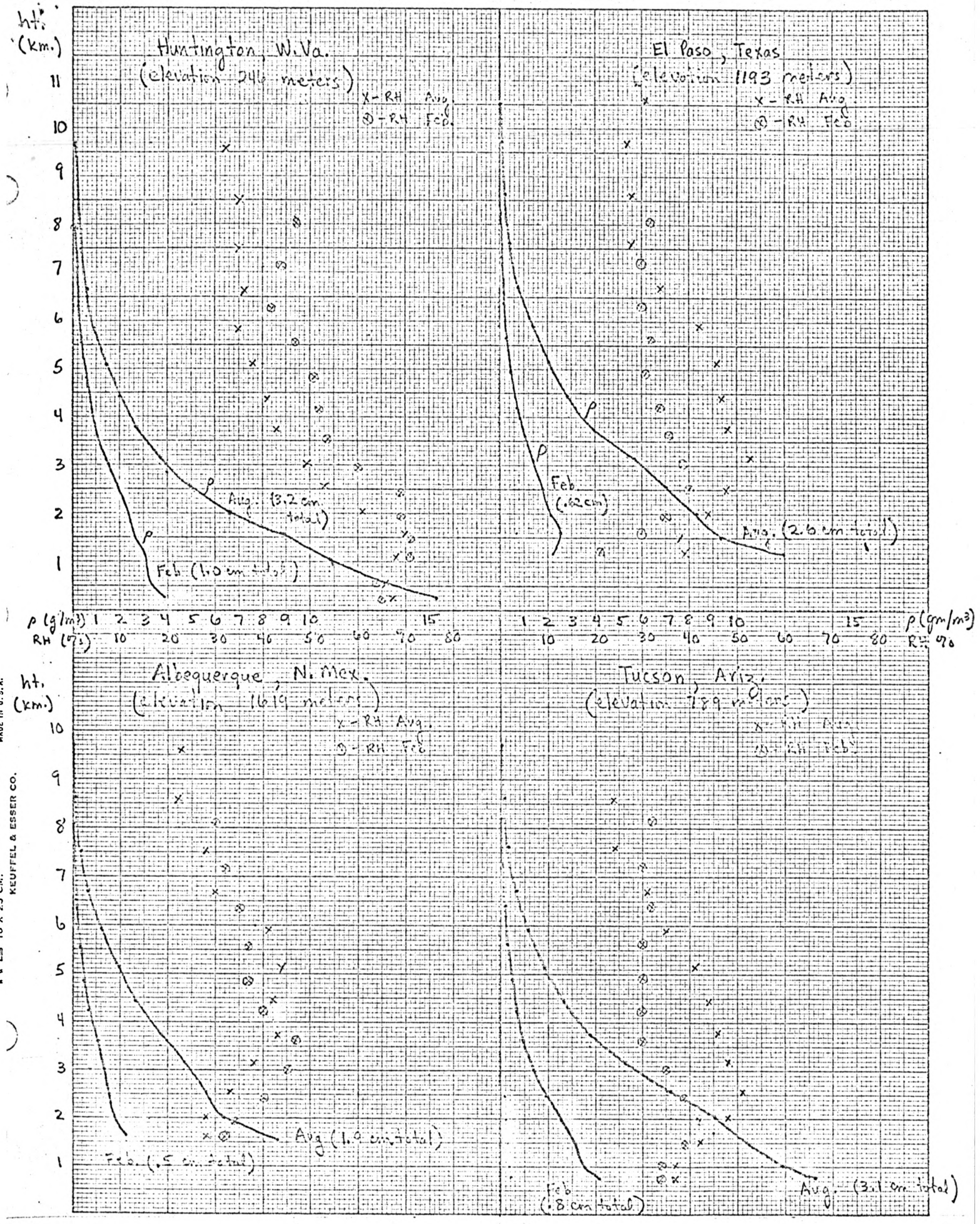

Fig. 7 — Atmospheric water vapor profiles (monthly means, 1966).

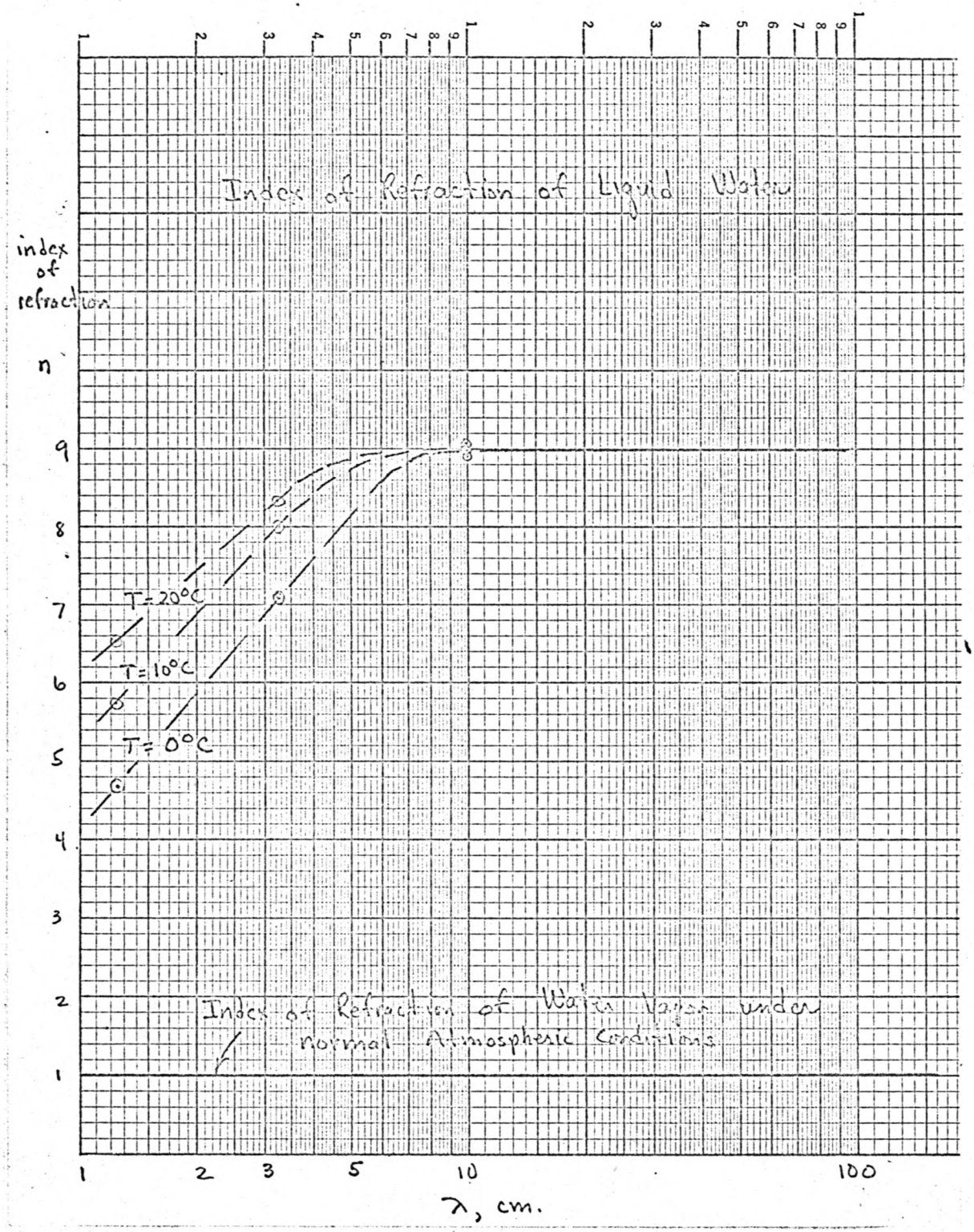

Fig. 8 — Index of refraction of water vs. wavelength.

Fig. 9 — Atmospheric water vapor spectra

T_B: Brightness temperature

τ : Opacity

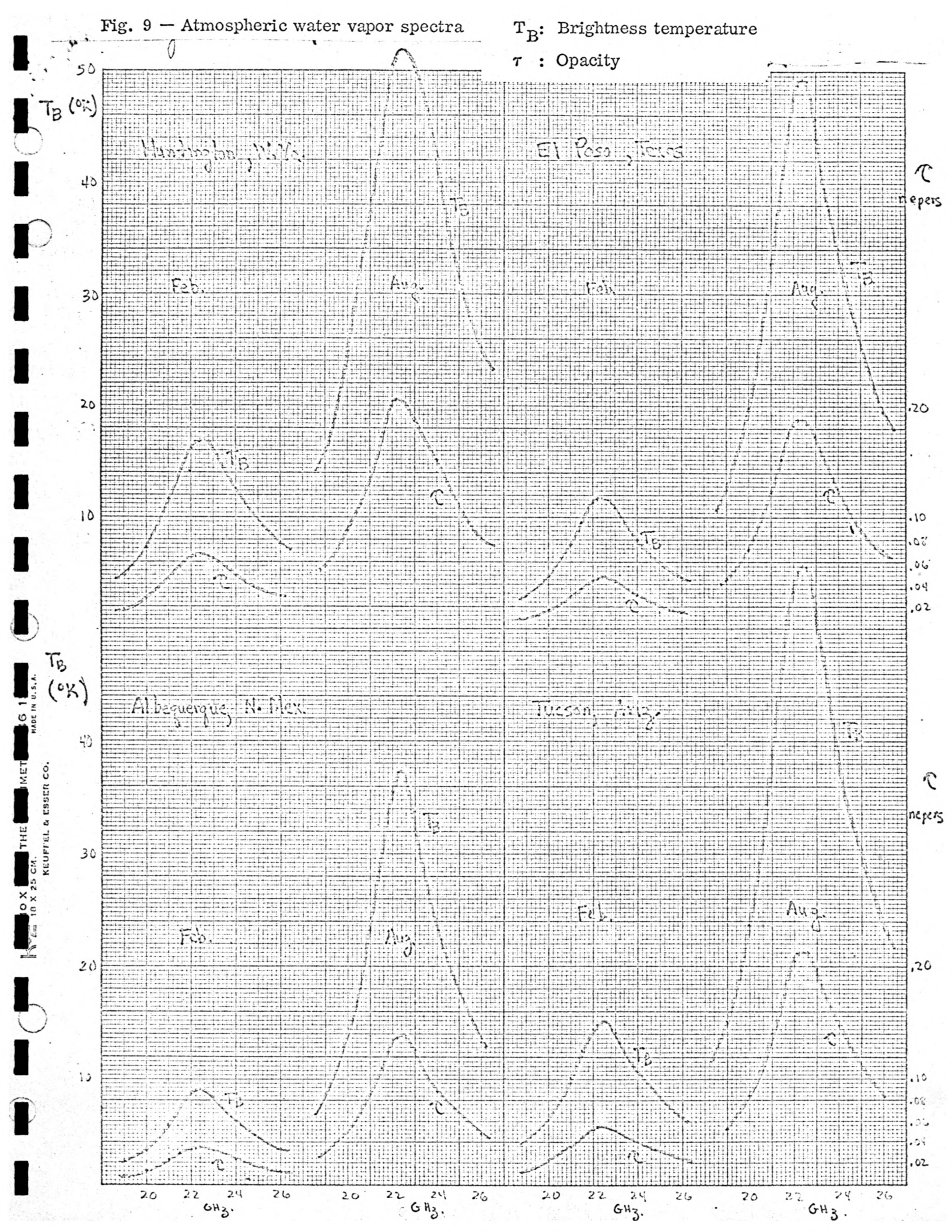

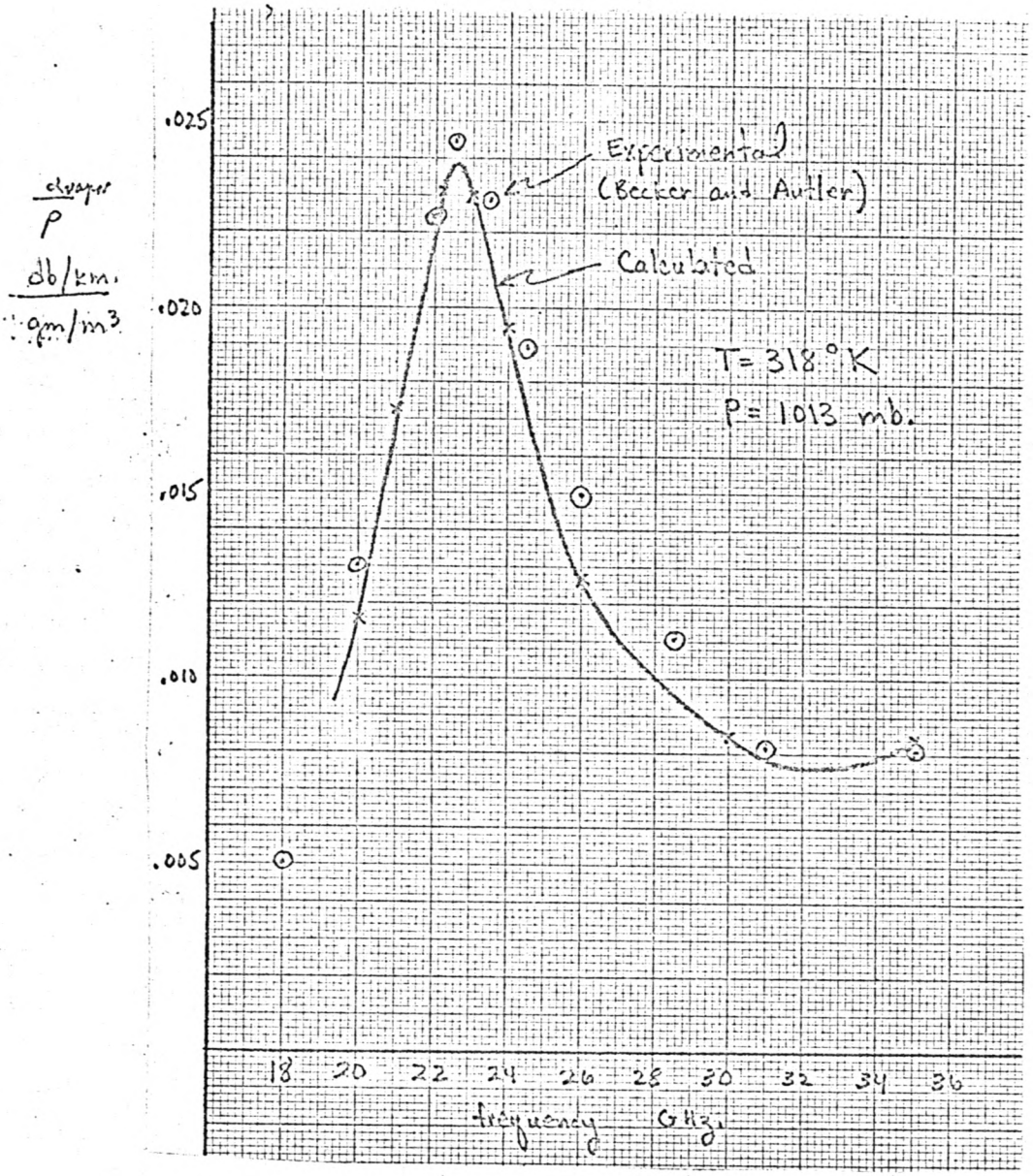

Fig. 10 — Water vapor absorption coefficient.

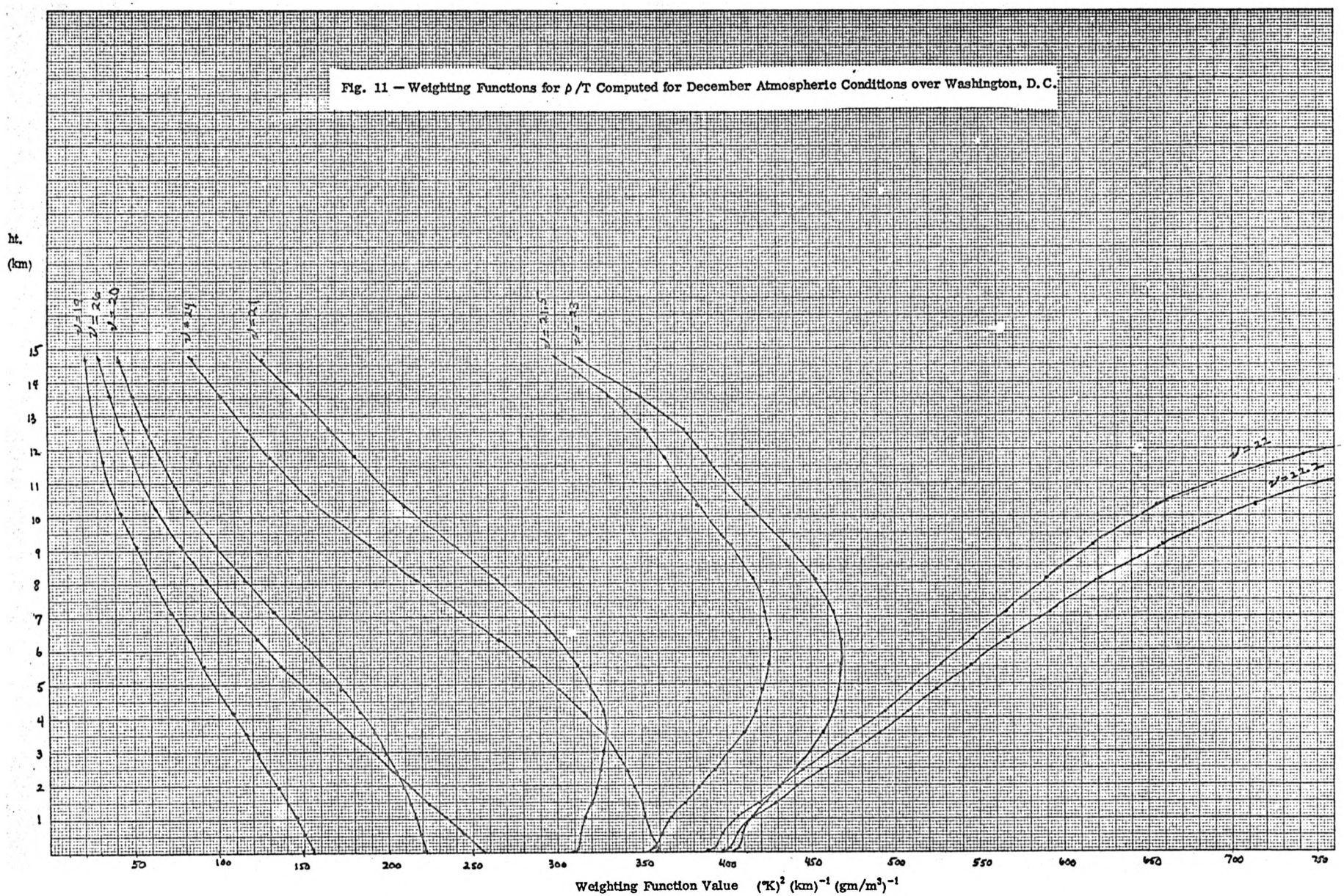
Fig. 11 — Weighting Functions for ρ/T Computed for December Atmospheric Conditions over Washington, D.C.
ht.
(km)
15
14
13
12
11
10
9
8
7
6
5
4
3
2
1
50
100
150
200
250
300
350
400
450
500
550
600
650
700
750
Weighting Function Value (°K)² (km)⁻¹ (gm/m³)⁻¹

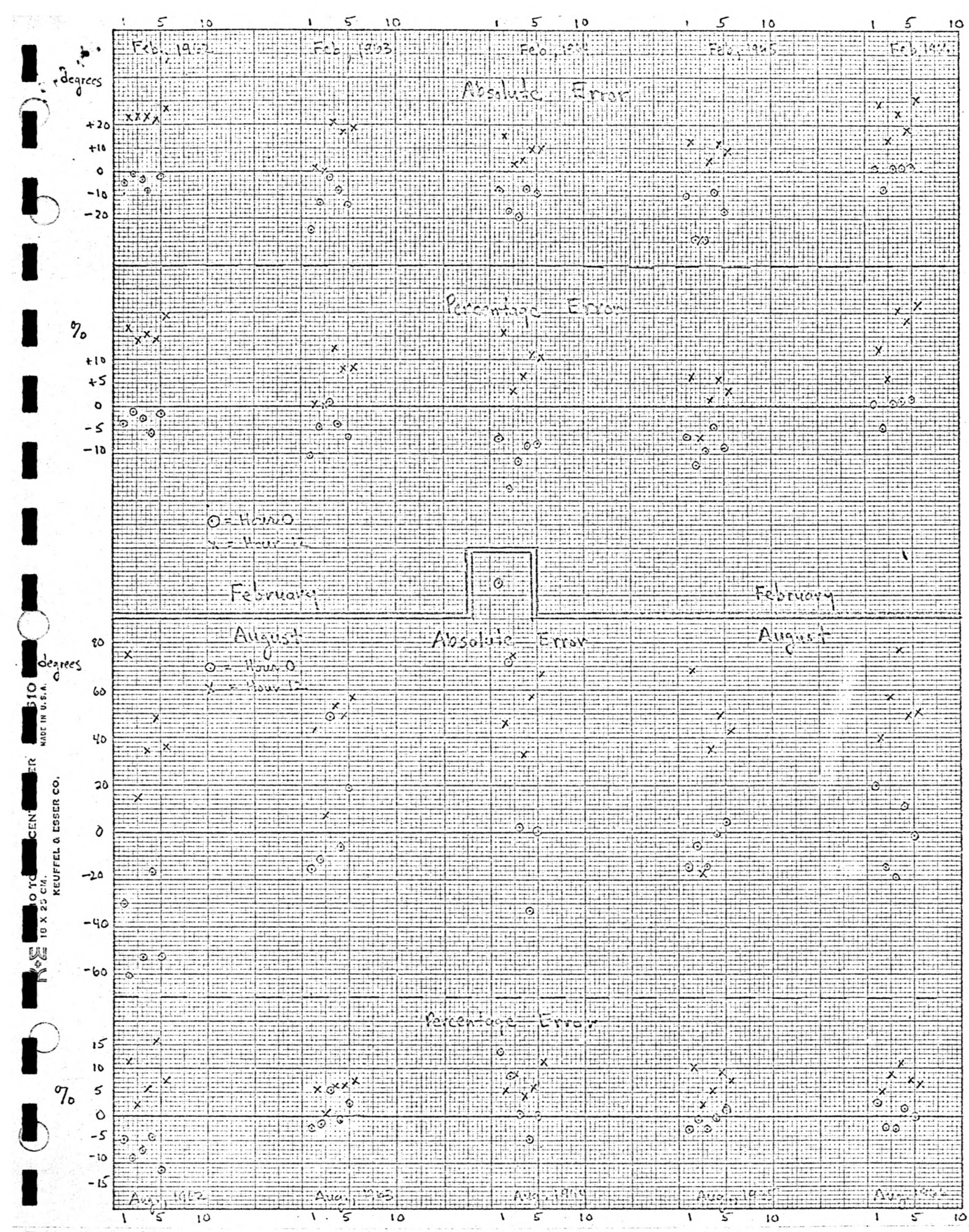

Fig. 12 — Errors in predicting phase delay due to water vapor (Tucson).

APPENDIX 1

The Dispersive Effect of the 1.35 cm Water Vapor Resonance Line on the Refractive Index of Air

The refractive index n and absorption coefficient α in decibels per kilometer are related to the complex dielectric constant, $\epsilon = \epsilon_r - i\epsilon_i$ by [1]

$$n = \sqrt{\epsilon_r}$$

$$\alpha = \frac{2\pi}{\lambda} \cdot 10^6 \epsilon \cdot \log_{10} e \tag{1}$$

where λ is in cm and it has been assumed $n^2 \approx 1$ (valid for air since $n_{air} \approx 1.0003$).

In the region near a resonant frequency ν_0, quantum mechanical calculations of the complex dielectric constant yield [1]

$$\epsilon_r - 1 = \frac{A\nu_0}{2}\left[\frac{\nu_0 - \nu}{\Delta\nu^2 + (\nu - \nu_0)^2}\right] \tag{2}$$

$$\epsilon_i = \frac{A\nu_0}{2}\left[\frac{\Delta\nu}{\Delta\nu^2 + (\nu\ \nu_0)^2}\right] \tag{3}$$

where A is a dimensionless constant and $\Delta\nu$ is the line breadth constant assumed due to collisions and small compared to ν_0.

Combining (1), (2), and (3) with $\lambda\nu = c$ yields

$$\epsilon_r - 1 = \frac{10^{-6}}{2\pi \log_{10} e}\left(\frac{c}{\Delta\nu}\right)\left(\frac{\nu_0}{\nu} - 1\right)\alpha \tag{4}$$

For water vapor $\left(\frac{c}{\Delta\nu}\right)$ is determined experimentally [2] as .087 cm^{-1}.
Combining this with the other constants in (4):

$$\epsilon_r - 1 = (3.12 \times 10^{-6})\left(\frac{\nu_0}{\nu} - 1\right)\alpha$$

and the refractive index is

$$n = \sqrt{\epsilon_r} = 1 + 1.56 \times 10^{-6} \left(\frac{\nu_0}{\nu} - 1 \right) \alpha$$

or

$$n - 1 = 1.56 \times 10^{-6} \left(\frac{\nu_0}{\nu} - 1 \right) \alpha \qquad (5)$$

where α is attenuation in dB/km. Equation (5) for (n - 1) as a function of frequency is plotted in figure A-1. Values of α from [2] were used and are also plotted in this figure. The values of α shown in the figure are typical for atmospheric conditions. It is seen from the figure than n differs from unity by less than 10^{-7} as a result of water absorption.

The standard deviation in n due to changing meteorological conditions varies from 10^{-6} to $25 \cdot 10^{-6}$ [3] and is approximately two orders of magnitude larger than the variation in n due to dispersion at 1.35 cm.

References - Appendix 1

[1] Van Vleck, J. H., "The Relation Between Absorption and Dispersion," Chapter 8 of Propagation of Short Radio Waves, McGraw Hill (1951).

[2] Bean, B. R., and E. J. Dutton, Radio Meteorology, NBS Monograph 92 (1966).

[3] Bean, B. R., J. D. Horn, and A. M. Ozanich, Jr., Climatic Charts and Data of the Radio Refractive Index for the United States and the World, NBS Monograph 22 (1960).

APPENDIX 2

Relation Between Water Vapor Density, Relative Humidity, and Temperature

[Reference: Hess, S. L., Introduction to Theoretical Meteorology, section 4.7, c. 1959, Holt, Rinehart and Winston.]

The water vapor mixing ratio, w, is the ratio of the mass of water vapor present to the mass of dry air containing the vapor:

$$w = \frac{\rho_v}{\rho_d} = \epsilon \frac{e}{P - e} \approx \epsilon \frac{e}{P} \tag{1}$$

where ρ_v = vapor density

ρ_d = dry air density

e = partial pressure due to vapor

P = total pressure

ϵ = ratio of the molecular weights of water and dry air

The saturation mixing ratio, w_s, is

$$w_s = \epsilon \frac{e_{sat}(T)}{P} \tag{2}$$

where $e_{sat}(T)$ is the vapor saturation pressure at temperature T. Relative humidity RH, is the ratio of w to w_s expressed in percent:

$$RH = 100 \frac{w}{w_s} \tag{3}$$

Combining (1), (2), and (3)

$$\rho_v = .01\, RH \frac{\epsilon\, e_{sat}(T)}{P} \rho_d \tag{4}$$

P and ρ_d may be eliminated from (4) by applying the ideal gas law

$$PV = NRT \tag{5}$$

Using (5), (4) becomes

$$\rho_v = .01\,RH\,\frac{\epsilon\, e_{sat}(T)}{T}\,\frac{\rho_d V}{N}\cdot\frac{1}{R}$$

$$= .01\,RH\,\frac{m_d}{R}\,\frac{\epsilon\, e_{sat}(T)}{T} \qquad (6)$$

where m_d = molecular weight of dry air

= 28.966 up to 60 km

R = gas constant

Inserting numerical values into (6) yields for altitudes of 60 km or less

$$\rho_v = 2.17\,\frac{RH\, e_{sat}(T)}{T} \qquad (7)$$

where ρ_v = vapor density in grams per cubic meter.

$e_{sat}(T)$ = vapor saturation pressure in millibars.

T = temperature in degrees Kelvin

RH = relative humidity in percent.

A plot of the function $2.17\,\frac{e_{sat}(T)}{T}$ is shown in figure A-2. Values of $e_{sat}(T)$ were taken from the Handbook of Chemistry and Physics.

Note that the vapor density is a function of relative humidity and temperature only and does not depend upon pressure.

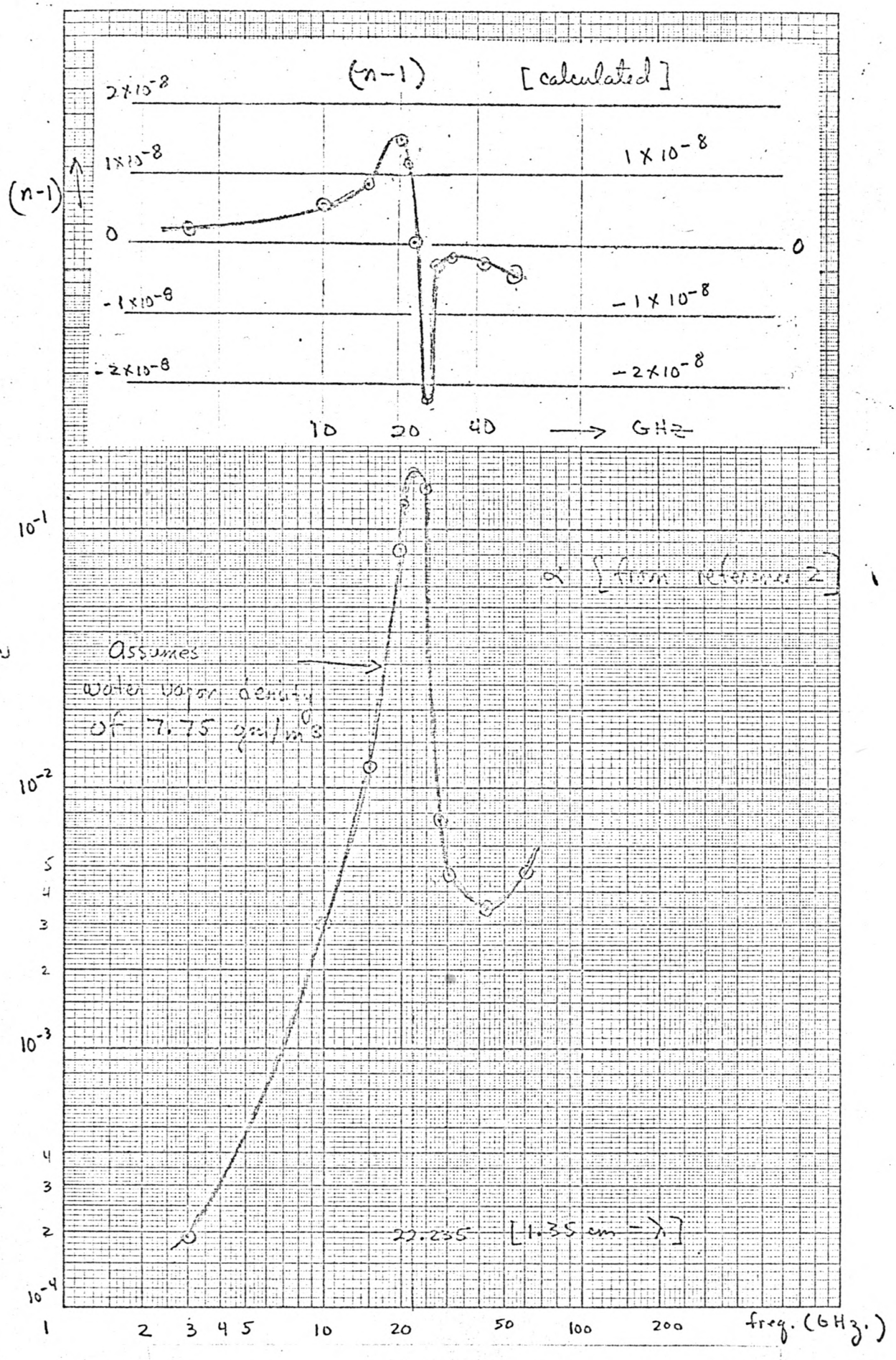

Fig. A-1 — Absorption and dispersion due to water vapor.

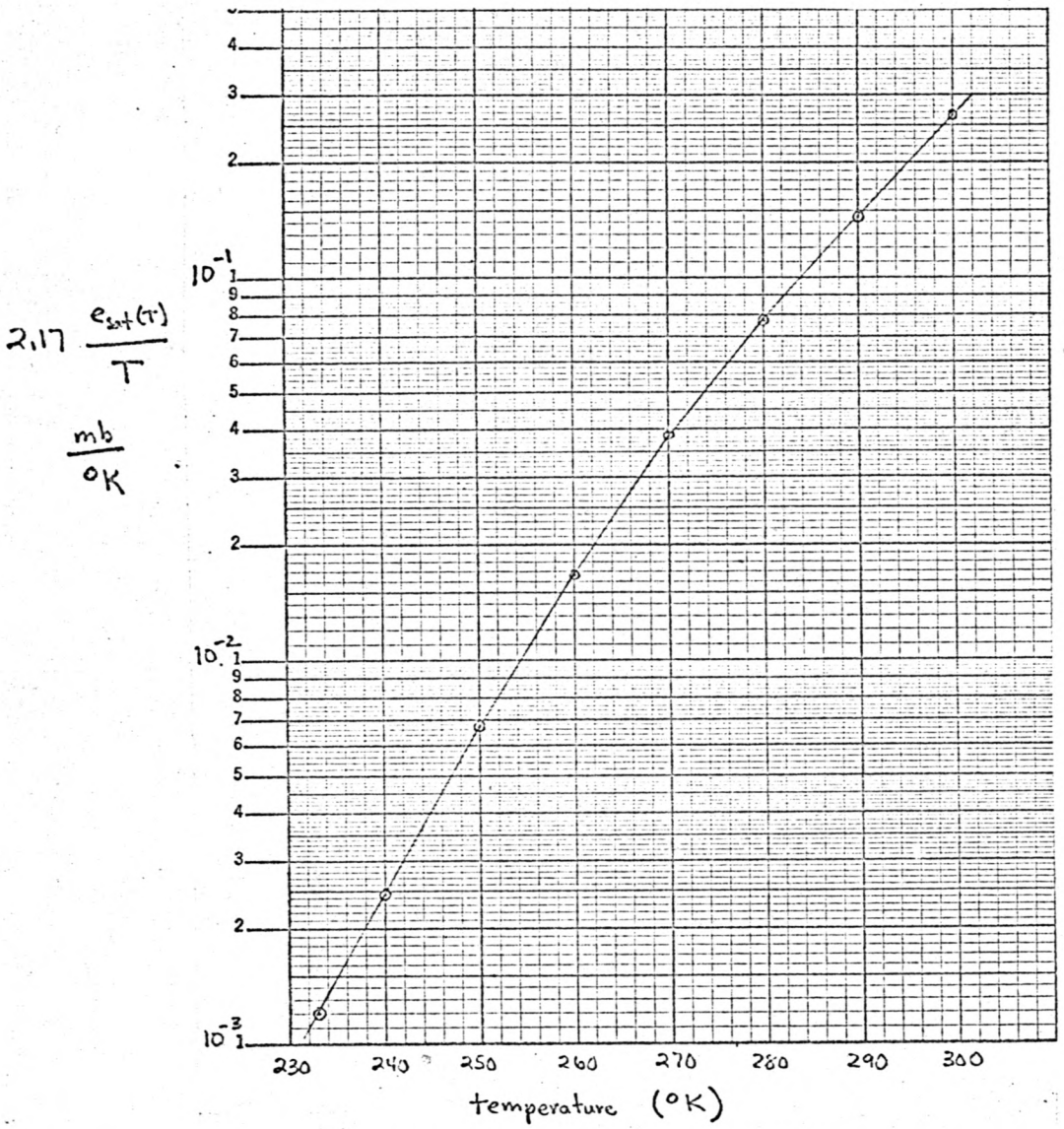

Fig. A-2 — The function 2.17 $\frac{e_{sat}(T)}{T}$